Independence of interrupted coarsening on initial system order: ion-beam nanopatterning of amorphous versus crystalline silicon targets

Independence of interrupted coarsening on initial system order: ion-beam nanopatterning of amorphous versus crystalline silicon targets

J Muñoz-García[1], R Gago[2], R Cuerno[1], J A Sánchez-García[2], A Redondo-Cubero[3], M Castro[4] and L Vázquez[2]

[1] Departamento de Matemáticas and Grupo Interdisciplinar de Sistemas Complejos (GISC), Universidad Carlos III de Madrid, Avenida de la Universidad 30, E-28911 Leganés, Spain
[2] Instituto de Ciencia de Materiales de Madrid, Consejo Superior de Investigaciones Científicas, E-28049 Madrid, Spain
[3] Instituto Tecnológico e Nuclear, Instituto Superior Técnico, Universidade Técnica de Lisboa, 2686-953 Sacavém, Portugal
[4] GISC and Grupo de Dinámica No Lineal (DNL), Escuela Técnica Superior de Ingeniería (ICAI), Universidad Pontificia Comillas de Madrid, E-28015 Madrid, Spain

E-mail: javiermunozgarcia@gmail.com

Abstract

Interrupted coarsening (IC) has recently been identified as an important feature for the dynamics of the typical length-scale in pattern-forming systems on surfaces. In practice, it can be beneficial to improve pattern ordering since it combines a certain degree of defect suppression with a limited increase in the typical pattern wavelength. However, little is known about its robustness with respect to changes in the preparation of the initial system for cases with potential applications. Working in the context of nano-scale pattern formation by ion-beam sputtering (IBS), we prove that IC properties do not depend on sample preparation. Specifically, interface dynamics under IBS is quantitatively compared on virgin amorphous and crystalline silicon surfaces, using 1 keV Ar^+ ions at normal incidence where nanodot pattern formation is triggered by concurrent co-deposition of Fe atoms during processing. Atomic force microscopy shows that dot patterns with similar spatial order and dynamics are obtained in both cases, underscoring the key dynamical role of the amorphous surface layer produced by irradiation. Both systems have been quantitatively described by an effective interface equation. We employ a new procedure based on the linear growth of the initial surface correlations to accurately estimate the equation coefficients. Such a method improves the predictive power of the interface equation with respect to previous studies and leads to a better description of the experimental pattern and its dynamical features.

(Some figures may appear in colour only in the online journal)

1. Introduction

The self-organized evolution of patterns that emerge under far-from-equilibrium conditions in dynamical systems is a complex phenomenon to which much attention has been devoted for a number of years [1], with particular attention being given lately to the novel kinetic conditions that occur at the nano-scale [2, 3]. Actually, mostly in the context of thin film growth by molecular beam epitaxy (see [4] for a recent review), much work has been done that has recently

led to the formulation of a general criterion to classify the forms of evolution in time t for the typical length-scale ℓ that characterizes a given pattern [5, 6]. These types of evolution can encompass well-known modes [1], from coarsening, in which power-law behavior ensues of the form $\ell(t) \sim t^n$, with n being a value with universality properties, to spatiotemporal chaos in which the late time pattern becomes completely disordered and ℓ ceases to be a significant description of the system. Within this classification, a novel behavior was predicted that has been termed interrupted coarsening (IC), in which coarsening in wavelength occurs, but only up to a time determined by system interactions. Although in the initial formulation of IC [5, 6] the amplitude of the pattern grows indefinitely with time, a variant of IC in which amplitude growth is also arrested has recently been verified experimentally [7], indeed in nanopatterning experiments. Still, IC has also been invoked to account for pattern dynamics in macroscopic systems, as in the formation of giant aeolian sand dunes [8].

From the point of view of applications, coarsening has both positive and negative implications for the size and quality of the patterns that are produced. On the one hand, coarsening occurs through defect annihilation [9], which improves the order of the structures. On the other hand, it introduces differences between the expected size of the pattern based on the nominal values of experimental parameters and the values that are actually obtained, that are not just confined to the nanometric range as initially desired. In this context, IC can be beneficial by combining a certain degree of defect suppression with a bounded increase of the typical pattern wavelength.

In order to deepen our understanding of IC, an important question regarding its robustness with respect to changes in the experimental system is considered. Thus, one might wonder whether the same non-trivial dynamics still holds when preparing the latter in a different way while preserving the main interactions that are presumably responsible for the occurrence of IC. In this way, IC would be an emergent property of the dynamics, rather than being controlled by the protocol followed to prepare the system.

In the present work we have pursued such an inquiry in the case of nanopattern formation on the surface of solid targets by erosion through ion-beam sputtering (IBS). This technique, that has a great interest for applications in (opto)electronics for example [10], was the one employed in the IC experiments of [7]. Frequently, under IBS the top-most surface layer of the target becomes amorphous as a result of ion bombardment, even if the nanostructure core remains crystalline [11]. The formation of this amorphous layer is a property of silicon that is common to other semiconductors, but not for other materials like metals [11, 12]. This detrimental and unavoidable layer, together with other ion induced lattice defects, may reduce the applicability of IBS patterns, especially if high crystal quality is required. From the basic point of view, a natural question arises on the relevance of the amorphous layer to the occurrence of IC when comparing initial targets that, say, are crystalline or are already amorphous at the outset. There are qualitative studies on the independence of pattern formation on the crystallinity

of the initial surface for compound materials [13], and on the starting crystalline orientation for silicon targets [14]. In contrast, the goal of our work is to perform a quantitative study that allows us to assess the independence of IC on the type of initial system, through detailed comparison for both amorphous and crystalline silicon targets with an evolution equation that presents IC. Such an equation has a large degree of universality, having been found in a number of different contexts, from growth of amorphous thin films [15], to ion-beam erosion [16–18], to macroscopic patterns in snow fields, for example [19].

2. Experiments

As is well documented in the literature [10], ripple [20] and dot [21] morphologies are typically produced by IBS when employed on amorphous materials or on crystalline surfaces that amorphize upon ion bombardment, as in single crystal semiconductors. For ion energies between hundreds of eV and a few keV, the structures produced have typical sizes of a few tens of nanometers.

For monoelemental semiconductors like silicon, nanodot patterns produced at near-normal ion incidence are triggered by the incorporation of metal impurities (typically, Fe or Mo) during processing [22, 23]. If the Fe is not supplied concurrently during the irradiation the surface will finally flatten. The smoothing process after pattern formation (with metal co-deposition) has been studied by several groups (see for example [24, 25]). In our present experiments we have employed the incorporation of iron impurities to induce nanodot patterns on silicon surfaces. In particular, targets consisting of amorphous Si (a-Si) films with thickness $\simeq 1.2\ \mu$m were grown at room temperature on Si(001) substrates by DC magnetron sputtering in a pure Ar atmosphere. In order to achieve a-Si films with a roughness σ, defined as the root-mean-square deviation of the surface, similar to that of the bare Si(100) substrate ($\sigma \simeq 0.2$ nm)—which will enable a precise comparison of the dynamics in the two systems—a relatively low discharge pressure (1×10^{-3} mbar) and power (25 W) were used in the growth process [26]. A reproducible structure (thickness and roughness) and the completely amorphous nature of the as-grown films were verified by *ex situ* spectroscopic ellipsometry measurements [27]. For pattern production, a-Si and crystalline Si(100) (c-Si) targets (size of 15×10 mm^2) were sputtered simultaneously with 1 keV Ar$^+$ ions at normal incidence. In order to ensure equivalent ion bombarding conditions (flux, dose, etc) on both targets, they were mounted at the center of the sample holder, which was rotated continuously during the irradiation at 10 rpm. Iron impurities were incorporated by concurrent irradiation of a steel mask with an inner hole diameter of 12 mm attached to the top of the samples. The ions were extracted from a commercial 3 cm beam-diameter CSC Kaufman-type ion gun (Veeco©) located 20 cm away from the target. The current density on the sample was measured prior to irradiation with a Faraday cup, and set to $\simeq 300\ \mu$A cm^{-2}. The erosion rate during IBS was evaluated with a Dektak 150 (Veeco©)
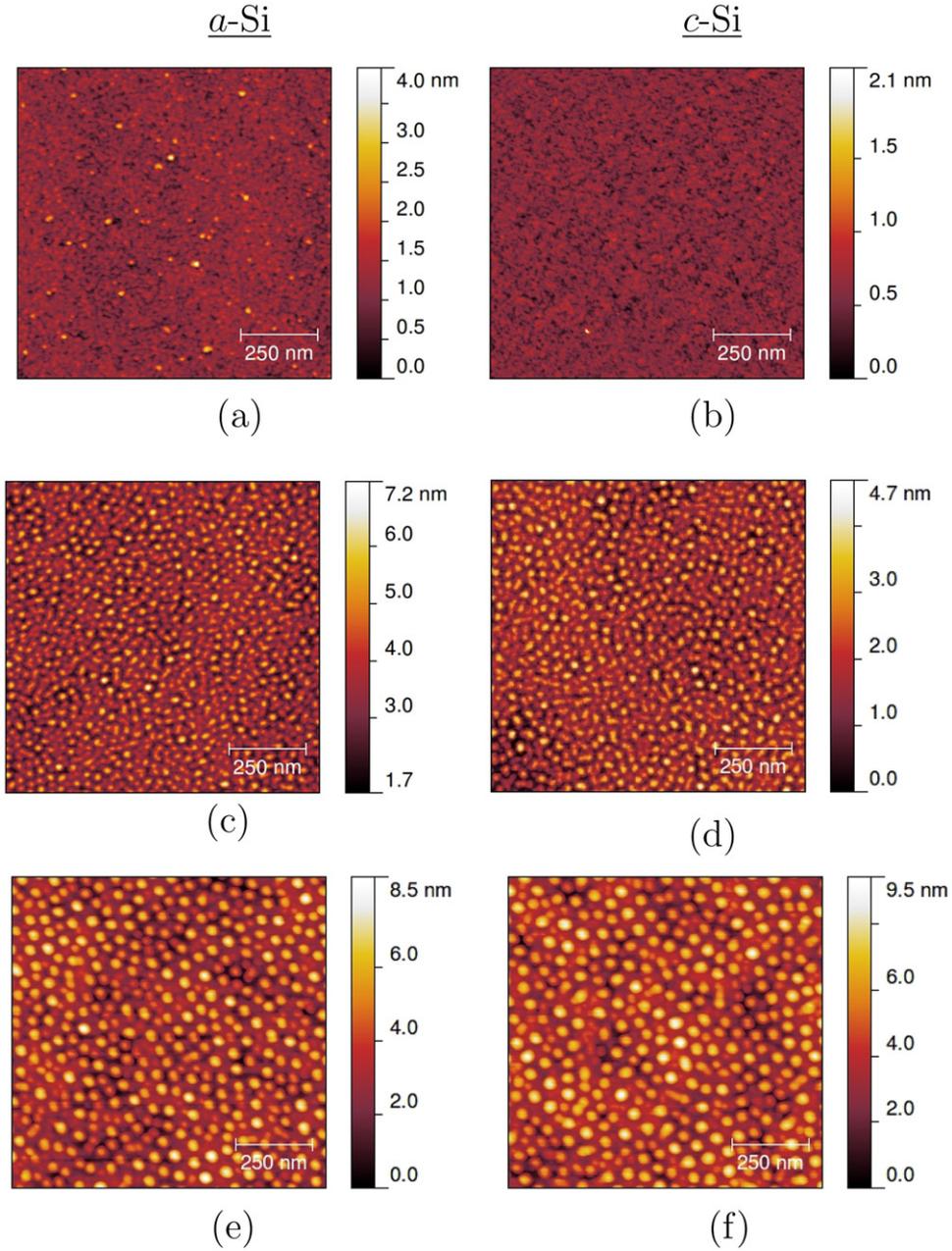
Figure 1. AFM 1×1 μm^2 images showing the evolution of the initial flat a-Si (left column) and c-Si (right column) surfaces before ((a), (b)) and after irradiation with 1 keV Ar$^+$ at 7.5 min ((c), (d)), and 46 min ((e), (f)). White scale bars represent 250 nm.

mechanical profiler. For this purpose, we measured the step created between the exposed part of the sample and the part covered by the Fe mask. These measurements yield a similar sputtering rate in a-Si and c-Si targets (18 nm min^{-1}). In order to avoid reaching the film/substrate interface in the case of a-Si films, the sputtering time was limited to approximately 1 h (i.e. ion fluence up to $\simeq 7 \times 10^{18}$ ions cm^{-2}). Note that the number of metal impurities can change dramatically the morphology of the resulting patterns [22, 28, 29, 23]. In our case, metal contaminants have been quantified by Rutherford backscattering spectrometry (RBS). Since both a-Si and c-Si targets were irradiated simultaneously, they showed a similar stationary Fe coverage (below 2×10^{15} atoms cm^{-2}), which was reached after just the first few minutes of irradiation.

The surface topographies before and after irradiation were imaged by *ex situ* atomic force microscopy (AFM) with Nanoscope IIIa equipment (Veeco©). Measurements were carried out in air with silicon cantilevers (model TESP from Bruker), with a nominal radius of 8 nm and an opening angle smaller than 52°, operating in tapping mode. For quantitative analysis, the global roughness σ and pattern wavelength (ℓ) were evaluated. The latter was extracted from the radial autocorrelation function [30] of the corresponding AFM images.

The morphological evolution of a-Si (left) and c-Si (right) targets under 1 keV Ar$^+$ bombardment is followed in figure 1. Panels (a), (b) show the pristine topographies of a-Si and c-Si targets, respectively, both displaying a relatively smooth

surface ($\sigma \simeq 0.2$–0.3 nm). After approximately 7.5 min of irradiation (figures 1(c), (d)), the formation of short-range hexagonal nanodot patterns is observed on both surfaces. The AFM images already suggest that the patterns induced on a-Si and c-Si surfaces display similar characteristics. Note that while the dot height and pattern wavelength values measured by the AFM are reliable, tip convolution issues may affect the measured horizontal distances close to the tip diameter. Therefore, tip convolution effects can lead to an overestimation of the dot diameter.

The surface dynamics is described quantitatively in figure 2, where the radial power spectral density (PSD) $S(\mathbf{k}, t) = \langle \hat{h}(\mathbf{k}, t)\hat{h}(-\mathbf{k}, t) \rangle$ (a), global roughness $\sigma(t)$ (b) and pattern wavelength $\ell(t)$ (c) are shown at different sputtering times. Here, $\hat{h}(\mathbf{k}, t)$ is the space Fourier transform of the height map $h(\mathbf{r}, t)$. Given the exact relation [30] between roughness and PSD $\sigma^2(t) = \int 2\pi k S(k, t)\,\mathrm{d}k$,[5] the small difference in spectral power between the starting a-Si and c-Si surfaces in figure 2(a) is seen to lie within the sample-to-sample variability for any of the two conditions (note the essentially identical values of $\sigma(t = 0)$ in figure 2(b)); similar considerations apply for longer times. After 7.5 min of sputtering, the PSD curves show a peak revealing the existence of a characteristic scale in the morphology, related to the pattern wavelength as $k_{\max} = 2\pi/\ell$. Specifically, at 7.5 min such a local maximum occurs for k values close to 0.17 nm^{-1}, corresponding to 36 nm, that is the typical size of the dots that appear and arrange into short-range order in figures 1(c) and (d). After pattern onset, the peak in the radial PSD shifts towards smaller k values (larger distances), suggesting coarsening behavior for ℓ (note, for example, the larger dot sizes in figures 1(e) and (f)). The similarity between the radial PSD curves for the two a-Si and c-Si targets at each specific time is striking. This behavior implies equivalent pattern characteristics and dynamics for both surfaces, which also applies to the order of the pattern (size of hexagonal dot domains), as derived from the width of the $S(k)$ peaks [30, 31].

Further important properties of the surface evolution are quantified in figures 2(b) and (c), with nearly a one to one correlation between the results from a-Si and c-Si (considering experimental deviations). Figure 2(b) (resp. 2(c)) shows an initial increase of the roughness (resp. ℓ, namely coarsening) followed by stabilization to a stationary state. The crossover towards saturation in σ and ℓ is achieved after around 30 min of sputtering. The similar trends in $\sigma(t)$ and $\ell(t)$ indicate correlation between the typical inter-dot distance and their height. The evolutions shown in figure 2 (see below for details about the theoretical results) are similar to those reported previously by the present authors for irradiations under different conditions on Si(100) (see for example [32, 33]). In turn, these results differ slightly from those reported in [7]. This can be related to the pattern formation process, since the only difference here with respect to the experiments in [7] is the simultaneous rotation of the
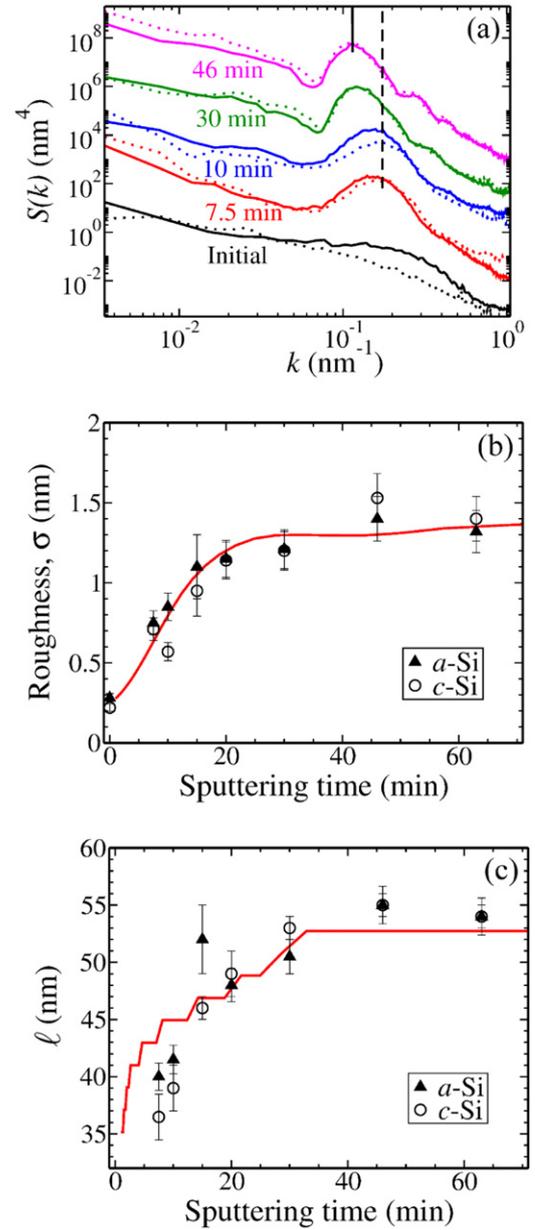
Figure 2. (a) Radial PSD curves $S(k)$ extracted from the AFM images of the initial flat a-Si (solid lines) and c-Si (dotted lines) surfaces sputtered with 1 keV Ar$^+$ for different times (see labels). The spectra at different times have been shifted vertically for clarity. The vertical dashed and solid lines in (a) indicate the modes that maximize $S(k)$ at 7.5 min and 46 min, respectively. Time evolution of the global roughness σ (b) and dot wavelength ℓ (c). The red solid lines in (b) and (c) represent the theoretical prediction obtained by numerical integration of equation (1).

sample holder. Sample rotation results in a slightly lower content of metal impurities as assessed by RBS. Since the metal content is related to the roughening process leading to the pattern formation [22, 28, 29, 23], the lower metal content may be responsible for structures with smaller size, as derived from the smaller saturation roughness (height) and wavelength (width) in figure 2. The similarity in the pattern formation and dynamics between a-Si and c-Si supports the relevant role of the surface amorphous layer for the pattern

formation. The negligible influence of pre-existing amorphous material in the dynamics can also be explained by the fact that crystalline Si becomes amorphous for small ion doses of 10^{14}–10^{15} ions cm^{-2} [11], which implies irradiations of just a few seconds under our present working conditions.

3. Theoretical description and comparison with experiments

A successful approach to describe IBS pattern formation is based on continuum models. Traditionally, the process was understood as the interplay between the unstable dependence of the sputtering yield on local surface curvature and stabilizing relaxation mechanisms due to surface diffusion, as expressed in the continuum equation put forward in a seminal work by Bradley and Harper (BH) [34]. However, this phenomenon is far from being completely understood. New experimental evidence and theoretical works suggest that additional mechanisms should be considered to successfully describe the pattern formation. For example, it has been shown that mass redistribution [35, 36], contamination [37, 24], or stress driven solid flow [38–40] can play relevant roles in this context.

In [18, 41, 42] a continuum description was proposed in which the evolution of the density of mobile material at the surface was coupled with surface-confined viscous flow, exploiting a direct analogy with the so-called 'hydrodynamic models' of pattern formation on aeolian sand dunes [43, 44]. In the present case of an ion-beam that is perpendicular to the initial target orientation, the surface dynamics can be described by the following effective equation,

$$\frac{\partial h}{\partial t} = -\nu\nabla^2 h - \mathcal{K}\nabla^4 h + \lambda_1(\nabla h)^2 - \lambda_2\nabla^2(\nabla h)^2, \quad (1)$$

where $\nu, \mathcal{K}, \lambda_1, \lambda_2$ are positive coefficients depending on phenomenological parameters. If $\lambda_2 = 0$, equation (1) reduces to the Kuramoto–Sivashinsky equation [45, 46], which on large domains produces a chaotic cellular structure with a fixed characteristic wavelength given by the linear instability. On the other hand, if $\lambda_2 \neq 0$ equation (1) produces a pattern of paraboloids which coarsen in time and display short-range order. The latter formalism (or condition) has been successfully applied to quantitatively describe coarsening and stabilization occurring during the dynamics of nanodot pattern formation on single crystal silicon surfaces [7]. It is also relevant to the IC dynamics of a number of different non-equilibrium systems, with typical scales from nanometers to meters, as mentioned above [15, 16, 18, 19]. As analyzed in [18, 12, 7], equation (1) describes an IC process in which a dot pattern forms and coarsens during a transient time; for longer times, the pattern reaches stationary values for its wavelength and amplitude at small to intermediate distances, while the morphology becomes disordered and rough at larger distances. In the context of IBS, equation (1) was originally formulated for the case of monoelemental amorphous or amorphizable materials; however, it also reproduces the pattern dynamics accurately when the destabilizing effect is enhanced by surface contamination [7], as in the present

experimental setup. The validity of this continuum description is due to the fact that equation (1) contains the most relevant terms compatible with the morphological instability, symmetry, conservation laws, and coarsening dynamics exhibited by the physical system considered. Actually, this equation can also be derived for the present case under these general assumptions, via the general formalism based on multiple scale arguments proposed in [47].

Here we improve the methodology from [7] in order to compare the evolution of a-Si and c-Si targets with the theoretical description provided by equation (1). Approximate analytical predictions from [12] and appropriate experimental observables allow us to estimate the values for the coefficients entering equation (1), in order to reproduce quantitatively the experimental dynamics shown in figures 2(b) and (c). In particular, at the early-stage for pattern formation, the linear instability wavelength is constant and given by $\ell_l = 2\pi(2\mathcal{K}/\nu)^{1/2}$. After the coarsening process, the asymptotic pattern wavelength differs from this value and remains constant. Its value is given by $\ell_f = (32\lambda_2/\lambda_1)^{1/2}$ (see [12]). Furthermore, the stationary dot amplitude A is proportional to ν/λ_1, specifically $A_f = 1.25\nu/\lambda_1$. For a slightly perturbed planar surface, the time for instability onset is given by the inverse of the maximum value of the linear dispersion relation [1, 7]. However, as IC is the manifestation of the competition between small-scale and large-scale interactions, the role of the correlations and roughness of the initial substrate needs to be analyzed carefully. In our case, since the roughness of the initial morphology is relatively large ($\sigma \simeq 0.2$–0.3 nm) we introduce a novel procedure to perform a better estimation of the equation coefficients.

In the linear regime, before non-linear terms in equation (1) become non-negligible, the temporal evolution of the surface height in Fourier space $\hat{h} = \hat{h}(k, t)$ is given by

$$\frac{\partial \hat{h}}{\partial t} = \nu k^2 \hat{h} - \mathcal{K}k^4 \hat{h} = \omega_k \hat{h}, \quad (2)$$

where the linear dispersion relation is $\omega_k = \nu k^2 - \mathcal{K}k^4$. Hence, within the linear regime the exact PSD function reads $S(k, t) = S(k, 0)\exp(2\omega_k t)$, and the global roughness becomes

$$\sigma^2(t) = \int 2\pi k S(k, 0)\, e^{2\omega_k t}\, dk. \quad (3)$$

The power spectral density of the initial surface, $S(k, 0)$, is directly calculated from the initial surface morphology as measured by AFM, which is also used as the initial condition for our numerical simulations. Since the linear dispersion relation for equation (1) depends on ν and $\mathcal{K}$, we can obtain the values of these two coefficients for our experimental conditions through the measured roughness curve $\sigma(t)$, and equation (3). For instance, we consider the value of σ at 7.5 min. Since the ratio of $\mathcal{K}$ and ν are constrained by the observed value of the linear instability wavelength $\ell_l \simeq$ 36 nm, we obtain the value of ν in equation (3) as the one that leads to the observed value $\sigma(t = 7.5 \text{ min}) = 0.7$ nm. Thus, we get $\nu = 13.2$ nm^2 min^{-1}. Hence, in contrast to the way in which the coefficients were obtained in [7], here the measured global roughness and the initial PSD of the
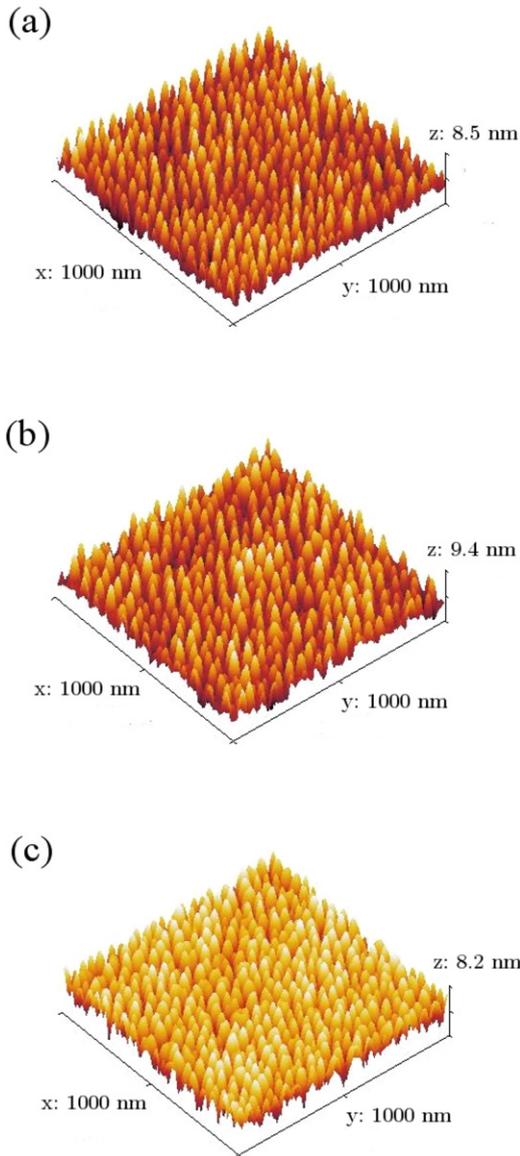
Figure 3. Three-dimensional views of the surface morphology of a-Si (a) and c-Si (b) targets irradiated for 46 min together with the corresponding numerical simulation (c) for the same time.

surface are required in order to completely determine all the coefficients appearing in equation (1).

From the experimental results, the final dot wavelength and amplitude are $\ell_\mathrm{f} \simeq 50$ nm and $A_\mathrm{f} \simeq 4$ nm, respectively. Using these values and those of ℓ_l and ν, we additionally obtain $\mathcal{K} = 207$ nm^4 min^{-1}, $\lambda_1 = 4.42$ nm min^{-1}, and $\lambda_2 = 291$ nm^3 min^{-1}. For these coefficient values, we have performed a numerical study of equation (1) using a fourth-order Runge–Kutta method and the improved spatial discretization introduced by Lam and Shin [48] for the non-linear terms. We have employed periodic boundary conditions, a spatial step $\Delta x = 1000/512$ nm, and time step $\Delta t = 10^{-4}$ min, checking that results do not differ significantly for smaller step values. This choice for Δx and Δt allows us to compare directly simulation and experimental length and time scales.

The simulated three-dimensional morphology obtained after 46 min is compared with the experimental ones in figure 3. Despite the fact that equation (1) depends only on height derivatives and can only predict dot patterns that are closely packed, the typical global size and height of the structures are very similar to the AFM measurements. These magnitudes have been further quantified for the simulated surfaces, results being depicted as solid lines in figures 2(b) and (c) at different times, together with the experimental data; agreement is excellent. Note that equation (1) reproduces not only the experimental values of the global roughness, initial wavelength, and final dot amplitude and wavelength, but also their complete evolutions, including the saturation time for both the global roughness and wavelength, which occurs after approximately 30 min. Moreover, even if the universality properties that occur in IC and other coarsening phenomena could lead us to expect agreement between equation (1) and experiments only at the largest scales, here the continuum description is able to describe experimental data faithfully down to the smallest significant time (instability onset) and length (linear dot wavelength) scales.

4. Conclusions

In summary, the evolution of the surface morphology of a-Si and c-Si during nanopattern formation by IBS has been studied quantitatively by AFM. Formation of self-organized nanodot patterns has been successfully induced on both targets, with very similar IC dynamics. This proves that IC does not depend sensitively on the type of initial target that we employ but is, rather, an intrinsic property of the dynamics of the amorphous surface layer that controls the system. Actually, the formation of this layer must occur in a time scale that is faster than the temporal scale of the pattern formation, which is of the order of some minutes, so that the global time evolution is similar for both a-Si and c-Si targets. All this suggests the interest of focusing future efforts (from theoretical to experimental, and computational) on the properties of the amorphous layer, in order to understand the basic physical processes controlling this promising route to nanostructuring.

Furthermore, we have compared the evolution of the a-Si and c-Si surfaces with that predicted by the effective continuum equation (1), for which the coefficient values have been obtained in a more systematic manner than in [7]. The method described in section 3 is based on the fact that the initial growth of the global roughness is mainly controlled by the linear terms. Thus, using the initial topographies and the value of σ at one initial stage we can obtain better estimates of the linear coefficients (ν and $\mathcal{K}$). This improves the predictive power of (1) and substantiates further its very validity to describe the present set of experiments. We believe that a more accurate description of the experimental results will help us to better control the nanopattern production using equation (1) as a theoretical guide. We also expect that the determined values of these coefficients for different experimental conditions (e.g. different material targets, etc) might give some clues about the main mechanisms operating during IBS pattern formation.

Acknowledgments

References

[1] Cross M and Greenside H 2009 *Pattern Formation and Dynamics in Nonequilibrium Systems* (Cambridge: Cambridge University Press)

[2] Cuerno R, Castro M, Muñoz-García J, Gago R and Vázquez L 2007 Universal non-equilibrium phenomena at submicrometric surfaces and interfaces *Eur. Phys. J. Special Top.* **146** 427

[3] Radons G, Rumpf B and Schuster G G 2010 *Nonlinear Dynamics of Nanosystems* (Weinheim: Wiley)

[4] Misbah C, Pierre-Louis O and Saito Y 2010 Crystal surfaces in and out of equilibrium: a modern view *Rev. Mod. Phys.* **82** 981–1040

[5] Politi P and Misbah C 2004 When does coarsening occur in the dynamics of one-dimensional fronts? *Phys. Rev. Lett.* **92** 090601

[6] Misbah C and Politi P 2009 Phase instability and coarsening in two dimensions *Phys. Rev.* E **80** 030106

[7] Muñoz-García J, Gago R, Vázquez L, Sánchez-García J A and Cuerno R 2010 Observation and modeling of interrupted pattern coarsening: surface nanostructuring by ion erosion *Phys. Rev. Lett.* **104** 026101

[8] Andreotti B, Fourrière A, Ould-Kaddour F, Murray B and Claudin P 2009 Giant aeolian dune size determined by the average depth of the atmospheric boundary layer *Nature* **457** 1120

[9] Bray A 1994 Theory of phase-ordering kinetics *Adv. Phys.* **43** 357

[10] Muñoz-García J, Vázquez L, Cuerno R, Sánchez-García J A, Castro M and Gago R 2009 Self-organized surface nanopatterning by ion beam sputtering *Toward Functional Nanomaterials* ed Z Wang (New York: Springer)

[11] Gnaser H 1999 *Low-Energy Ion Irradiation of Solid Surfaces* (Berlin: Springer)

[12] Muñoz-García J, Cuerno R and Castro M 2009 Coupling of morphology to surface transport in ion-beam-irradiated surfaces: normal incidence and rotating targets *J. Phys.: Condens. Matter* **21** 224020

[13] Fascko S, Bobek T, Kurz H, Dekorsy T, Kyrsta S and Cremer R 2002 Ion-induced formation of regular nanostructures on amorphous gasb surfaces *Appl. Phys. Lett.* **80** 130

[14] Gago R, Vázquez L, Plantevin O, Metzger T H, Muñoz-García J, Cuerno R and Castro M 2006 Order enhancement and coarsening of self-organized silicon nanodot patterns induced by ion-beam sputtering *Appl. Phys. Lett.* **89** 233101

[15] Raible M, Mayr S G, Linz S J, Moske M, Hänggi P and Samwer K 2000 Amorphous thin-film growth: theory compared with experiment *Europhys. Lett.* **50** 61

[16] Kim T C *et al* 2004 Kinetic roughening of ion-sputtered Pd(001) surface: beyond the Kuramoto–Sivashinsky model *Phys. Rev. Lett.* **92** 246104

[17] Castro M and Cuerno R 2005 Comment on kinetic roughening of ion-sputtered Pd(001) surface: beyond the Kuramoto–Sivashinsky model *Phys. Rev. Lett.* **94** 139601

[18] Castro M, Cuerno R, Vázquez L and Gago R 2005 Self-organized ordering of nanostructures produced by ion-beam sputtering *Phys. Rev. Lett.* **94** 016102

[19] Tiedje T, Mitchell Kevin A, Lau B, Ballestad A and Nodwell E 2006 Radiation transport model for ablation hollows on snowfields *J. Geophys. Res.* **111** F02015

[20] Navez M, Sella C and Chaperot D 1962 Étude de l'attaque du verre par bombardement ionique *C. R. Acad. Sci.* **254** 240

[21] Facsko S, Dekorsy T, Koerdt C, Trappe C, Kurz H, Vogt A and Hartnagel H L 1999 Formation of ordered nanoscale semiconductor dots by ion sputtering *Science* **285** 1551

[22] Ozaydin G, Özcan A S, Wang Y, Ludwig F, Zhou H, Headrick R L and Siddons D P 2005 Real-time x-ray studies of Mo-seeded Si nanodot formation during ion bombardment *Appl. Phys. Lett.* **87** 163104

[23] Macko S, Frost F, Ziberi B, Förster D F and Michely T 2010 Is kev ion-induced pattern formation on Si(001) caused by metal impurities? *Nanotechnology* **21** 085301

[24] Zhou J and Lu M 2010 Mechanism of fe impurity motivated ion-nanopatterning of Si(100) surfaces *Phys. Rev.* B **82** 125404

[25] Macko S, Frost F, Engler M, Hirsch D, Höche T, Grenzer J and Michely T 2011 Phenomenology of iron-assisted ion beam pattern formation on Si(001) *New J. Phys.* **13** 073017

[26] Redondo-Cubero A, Gago R and Vázquez L 2011 Ultrasmooth growth of amorphous silicon films through ion-induced long-range surface correlations *Appl. Phys. Lett.* **98** 011904

[27] Tompkins Harland G and Irene Eugene A 2005 *Handbook of Ellipsometry* (New York: William Andrew)

[28] Sánchez-García J A, Vázquez L, Gago R, Redondo-Cubero A, Albella J M and Czigány Zs 2008 Tuning the surface morphology in self-organized ion beam nanopatterning of Si(001) via metal incorporation: from holes to dots *Nanotechnology* **19** 355306

[29] Sánchez-García J A, Gago R, Caillard R, Redondo-Cubero A, Martin-Gago J A, Palomares F J, Fernández M and Vázquez L 2009 Production of nanohole/nanodot patterns on Si(001) by ion beam sputtering with simultaneous metal incorporation *J. Phys.: Condens. Matter* **21** 224009

[30] Zhao Y-P, Wang G-C and Lu T-M 2001 *Characterization of Amorphous and Crystalline Rough Surfaces: Principles and Applications* (San Diego: Academic)

[31] Ziberi B, Frost F, Höche T and Rauschenbach B 2005 Ripple pattern formation on silicon surfaces by low-energy ion-beam erosion: experiment and theory *Phys. Rev.* B **72** 235310

[32] Gago R, Vázquez L, Cuerno R, Varela M, Ballesteros C and Albella J M 2001 Production of ordered silicon nanocrystals by low-energy ion sputtering *Appl. Phys. Lett.* **78** 3316

[33] Gago R, Vázquez L, Plantevin O, Sánchez-García J A, Varela M, Ballesteros M C, Albella J M and Metzger T H 2006 Temperature influence on the production of nanodot patterns by ion beam sputtering of Si(001) *Phys. Rev.* B **73** 155414

[34] Bradley R M and Harper J M E 1988 Theory of ripple topography induced by ion bombardment *J. Vac. Sci. Technol.* A **6** 2390

[35] Madi C S, Anzenberg E, Ludwig K F and Aziz M J 2011 Mass redistribution causes the structural richness of ion-irradiated surfaces *Phys. Rev. Lett.* **106** 066101

[36] Norris S A, Samela J, Bukonte L, Backman M, Djurabekova F, Nordlund K, Madi C S, Brenner M P and Aziz M J 2011 Molecular dynamics of single-particle impacts predicts phase diagrams for large scale pattern formation *Nature Commun.* **2** 276

[37] Bradley R M and Shipman P D 2010 Spontaneous pattern formation induced by ion bombardment of binary compounds *Phys. Rev. Lett.* **105** 145501

[38] Castro M and Cuerno R 2010 Ion induced solid flow arXiv:1007.2144

[39] Cuerno R, Castro M, Muñoz-García J, Gago R and Vázquez L 2011 Nanoscale pattern formation at surfaces under ion-beam sputtering: a perspective from continuum models *Nucl. Instrum. Meth.* B **269** 894

[40] Castro M and Cuerno R 2012 Hydrodynamic approach to surface pattern formation by ion beams *Appl. Surf. Sci.* **258** 4171

[41] Muñoz-García J, Castro M and Cuerno R 2006 Nonlinear ripple dynamics on amorphous surfaces patterned by ion beam sputtering *Phys. Rev. Lett.* **96** 086101

[42] Muñoz-García J, Cuerno R and Castro M 2008 Coupling of morphology to surface transport in ion-beam irradiated surfaces: oblique incidence *Phys. Rev.* B **78** 205408

[43] Csahók Z, Misbah C, Rioual F and Valance A 2000 Dynamics of aeolian sand ripples *Eur. Phys. J.* E **3** 71

[44] Aste T and Valbusa U 2004 Surface instabilities in granular matter and ion-sputtered surfaces *Physica* A **332** 548

[45] Kuramoto Y and Tsuzuki T 1976 Persistent propagation of concentration waves in dissipative media far from thermal equilibrium *Prog. Theor. Phys.* **55** 356

[46] Sivashinsky G I 1977 Nonlinear analysis of hydrodynamic instability in laminar flames—I. Derivation of basic equations *Acta Astrounautica* **4** 1177

[47] Castro M, Muñoz-García J, Cuerno R, García-Hernández M and Vázquez L 2007 Generic equations for pattern formation in evolving interfaces *New J. Phys.* **9** 102

[48] Lam C-H and Shin F G 1998 Improved discretization of the Kardar–Parisi–Zhang equation *Phys. Rev.* E **58** 5592